



Article

Assessing the Feasibility of Fabricating Thermoplastic Laminates from Unidirectional Tapes in Open Mold Environments

Basit Ali, Khaled Kadri , Maen Alkhader * , Wael Abuzaid , Mohammad A. Jaradat , Mohammed Mustafa and Mohamed Hassanien

Department of Mechanical Engineering, American University of Sharjah, Sharjah 26666, United Arab Emirates; b00056664@alumni.aus.edu (B.A.); wabuzaid@aus.edu (W.A.); mjaradat@aus.edu (M.A.J.); mmustafa@aus.edu (M.M.); b00049813@alumni.aus.edu (M.H.)

* Correspondence: malkhader@aus.edu; Tel.: +971-6-5152955

Abstract: The automation of the manufacturing processes of thermoplastic composite laminates has become dependent on open mold processes such as automated tape placement (ATP), which couples tape layering with in situ consolidation. The manufacturing parameters of ATP open mold processes, which comprise processing time, consolidation pressure and temperature, affect the bond strength between the plies and the quality of the laminates produced. Therefore, the effect of the manufacturing parameters should be characterized. This work experimentally evaluates the feasibility of fabricating thermoplastic laminates using an open mold process that reasonably models that of ATP. Glass fiber-reinforced polypropylene laminates are fabricated from unidirectional tapes under different consolidation periods, pressures, and temperatures. The bond quality in the produced laminates is assessed by measuring their interlaminar shear strength, which is measured using a short beam standardized shear test in conjunction with digital image correlation. Results show that consolidation can occur at temperatures slightly below the composite tapes' complete melting temperature, and consolidation times between 7 and 13 min can result in acceptable bond strengths. The results confirmed the feasibility of the process and highlighted its limitations. Analysis of variance and machine learning showed that the effect of process parameters on interlaminar shear strength is nonlinear.

Keywords: fiber-reinforced polymer composite; glass fiber polypropylene; fabrication; interlaminar shear strength; adaptive neuro-fuzzy inference system; analysis of variance



Citation: Ali, B.; Kadri, K.; Alkhader, M.; Abuzaid, W.; Jaradat, M.A.; Mustafa, M.; Hassanien, M. Assessing the Feasibility of Fabricating Thermoplastic Laminates from Unidirectional Tapes in Open Mold Environments. *J. Manuf. Mater. Process.* **2024**, *8*, 12. <https://doi.org/10.3390/jmmp8010012>

Academic Editor: Steven Y. Liang

Received: 8 December 2023

Revised: 28 December 2023

Accepted: 4 January 2024

Published: 6 January 2024



Copyright: © 2024 by the authors. Licensee MDPI, Basel, Switzerland. This article is an open access article distributed under the terms and conditions of the Creative Commons Attribution (CC BY) license (<https://creativecommons.org/licenses/by/4.0/>).

1. Introduction

Fiber-reinforced polymer (FRP) composites are increasingly used in a wide range of applications pertaining to aerospace, marine, infrastructure, and automotive industries [1–5]. The move towards FRP composites and the increasing demand for them have been motivated mainly by their high specific strength and stiffness as well as their ability to conform to complex shapes without the need for intensive subtractive machining. The demand for FRP composites extends to their two classes, which comprise thermoset and thermoplastic matrices. Traditionally, applications requiring substantial structural properties, particularly at high temperatures, have favored thermoset FRP composites [6], as thermosets provide higher stiffness and strength than those of conventional thermoplastics. However, the development of thermoplastic polymers with high melting temperatures approaching those of thermosets, e.g., poly-ether-ether-ketone (PEEK), has spurred a growing interest in utilizing thermoplastic FRP composites in structural applications [6–8], particularly because thermoplastic FRP composites are more ductile and easier to fabricate, repair, reform, and recycle [9–12].

The move towards thermoplastic FRP composites has motivated the automation of the fabrication processes of their laminates. Thermoplastic FRP laminates are conventionally

fabricated from unidirectional prepregs or tapes (UD tapes) comprising fibers embedded in thermoplastic polymeric matrices. Manufacturing a thermoplastic laminate typically involves stacking plies cut from UD tapes in a mold and subjecting them to heat and pressure for a specific duration. This process is performed at temperatures exceeding the uniform melting temperature of the plies' matrix. Accordingly, the molds used fully enclose the plies to prevent the flow of the melted matrix outside the mold. This process is highly dependent on time-consuming hand lay-up operations [6], and it can become costly when used with large parts as it would require large and expensive molds. To automate this process, a relatively new technique, namely automated tape placement (ATP) [13–16], has been proposed.

In ATP, UD tapes are simultaneously heated, layered, and in situ consolidated at temperatures that do not cause significant melting and flow in the plies' matrix. The absence of significant matrix flow eliminates the need for the volume-preserving closed molds associated with conventional closed mold processing techniques, which utilize temperatures that significantly exceed the plies' melting temperature. By using an open mold environment, the automated placement and consolidation of plies in ATP processes can occur at high rates (e.g., 80 mm/s [17]), allowing for the fabrication of laminates at higher rates than those achievable by conventional closed mold processes.

However, the temperature, pressure and layering rate used in ATP open mold processes affect the bond strength between the consolidated plies and the quality of the laminates produced [18]. Accordingly, enhancing the quality of the produced laminates is instrumentally dependent on characterizing the interactive effect of these process parameters on the strength of the formed inter-ply bonds [19]. Pioneering studies have shown that higher processing rates generally require higher processing temperatures to maintain bond quality, but optimum bonding is realized at lower processing rates [20]. However, excessive temperatures can cause damage to embedded fibers [19]. Consolidation pressure was observed to play a critical role in eliminating entrapped gaps between plies and facilitating heat transfer across plies' interfaces [21]. Reducing temperature gradients leads to better inter-ply bonds and increases the laminate shear strength [14]. The aforementioned efforts represent the available studies investigating the process parameters of ATP open mold processes. They are very limited compared to the number of studies investigating process parameters in closed mold techniques, which showed that process parameters can have nonlinear and synergistic effects on bond strength [22–25]. Similar effects can be expected to arise in open mold processes. Therefore, more efforts are needed to better characterize the effect of process parameters on bond quality in ATP open mold processes. Moreover, although open mold processes provide higher throughput than their closed mold counterparts do, the latter provide better inter-ply bonds [14,26]. Accordingly, two lingering questions remain regarding the feasibility of ATP/open mold processes and the potential for enhancing the laminates they produce by better characterizing the effect of their process parameters. This work aims to address these questions.

Limited studies in the literature have investigated the process parameters' effect in ATP open mold processes as experimental setups required for conducting such work are expensive and complex. For instance, robotic arms, dispensing heads, and heating elements such as torches or lasers are required [14,18,19]. In place of such a complex experimental setup, this work proposes using a simple setup that reasonably models ATP open mold processes. In this setup, layering speed is represented by a processing period such that faster layering speeds can be represented by shorter processing periods. Instead of torches or lasers, heating is applied through compacting steel platens that ensure temperature and pressure uniformity in the processed plies. The setup, which is described in detail in the next section, is used to investigate the feasibility of processing thermoplastic laminates at different temperatures, pressures, and processing periods. The inter-ply bond strength in the produced laminates is investigated at the different processing parameters by measuring the laminates' interlaminar shear strength using a short-beam standardized test and digital image correlation technique. Using the laminate fabrication setup and inter-ply bond

measuring techniques, this work aims to provide insights into the feasibility of open mold processes and the effect of their process parameters. Moreover, this work aims to quantify the relationship between process parameters and inter-laminar shear strength using statistical and machine learning techniques.

2. Materials and Methods

The methodology used in this work comprises two phases. First, laminates are prepared and consolidated using a carefully selected range of controlled process parameters in a setup that reasonably models ATP open mold processes. Second, the laminates are tested, and their mechanical properties, namely interlaminar shear strength (ILSS), are measured. ILSS strongly correlates to the bond quality between plies in composite laminates and has been widely used to represent inter-ply bond strength [2,27–29]. Therefore, it is chosen in this work to quantify the effectiveness of the open mold consolidation process.

Multiple thermoplastic FRP candidates could have been used to conduct this study. However, due to its low cost and availability, glass fiber-reinforced polypropylene (GFPP) was selected as a representative thermoplastic material. The glass fiber-reinforced polypropylene (GFPP) used in this work was provided by Imhotepcomposites, UK. It was supplied as rolls of unidirectional (UD) tapes. The properties of the GFPP UD tapes, as provided by the manufacturer, are summarized in Table 1.

Table 1. Geometric and mechanical properties of GFPP UD tapes.

Property	Value	Property	Value
Width	90 mm	Tensile Strength	452 (MPa)
Thickness	0.4 mm	Tensile Modulus (E_1)	21.8 (GPa)
Density	1.65 g/mm ³	Tensile strain to break	2.4%
Process temperature	180 °C	Flexural Strength	323 (MPa)
Fiber content	70 Wt%, 45 V%	Flexural Modulus	16 (GPa)

The fabrication of laminates is performed using a hot press in which plies are heated and pressed between two parallel platens for specific durations. The parallel platens represent the compaction wheel and support plate used in ATP open mold processes, while duration represents the processing time (i.e., layering rate). The temperature and pressure applied by the hot press as well as the processing time are selected to reasonably model the ATP open mold process.

The selection of the processing temperature, the most critical processing parameter, is motivated by the primary feature of ATP open mold processes: the lack of a volume-preserving enclosure. Utilizing an open mold process necessitates processing and consolidating the GFPP UD plies at temperatures below their uniform melting temperature to prevent them from flowing outside the compacting platens. Since the supplier did not provide the melting temperature of the acquired GFPP UD tapes, it was determined using dynamic mechanical analysis (DMA). A DMA system from TA instruments (DMA 3200), USA, was used to determine the complex modulus of the GFPP UD tapes at temperatures ranging between 30 °C and 180 °C. The storage and loss moduli (i.e., the components of the complex modulus) are presented in Figure 1. The storage modulus shows that the stiffness of the GFPP tapes decreases exponentially at temperatures exceeding 140 °C and approaches zero near the 150 °C mark; however, it totally diminishes (i.e., complete loss of stiffness) at a temperature of ~152 °C. Accordingly, the DMA results suggest that the uniform or complete melting of the GFPP matrix occurs around ~152 °C, which falls well within the range of polypropylene melting temperatures reported in the literature [30].

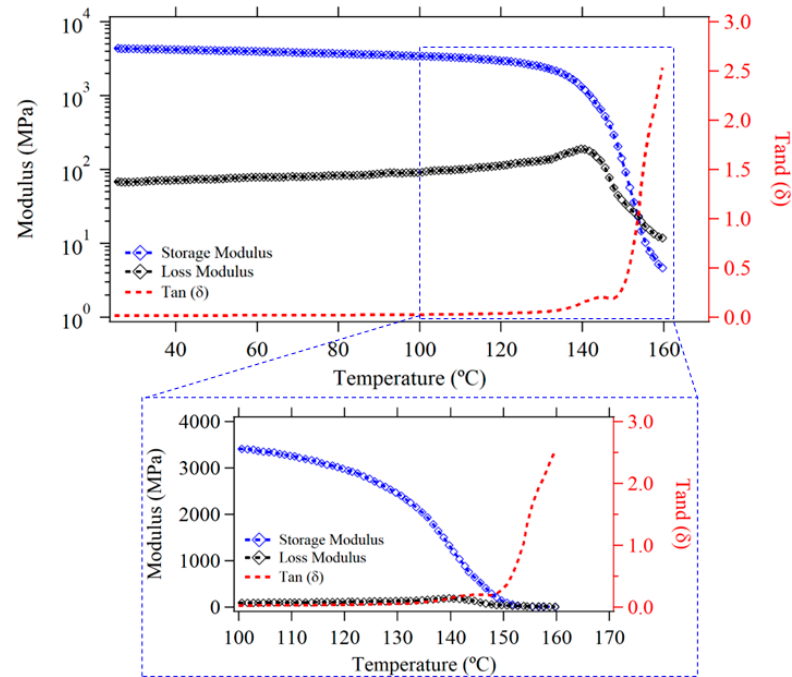


Figure 1. The storage and loss moduli of the GFPP UD tape, showing the properties along the direction of the fibers (longitudinal direction).

To verify the accuracy of the 152 °C uniform melting temperature determined via the DMA analysis, samples of GFPP were heated to a temperature of 152 °C in a Wabash hydraulic hot press (Wabash, IN, USA). The samples were sandwiched between temperature-resistant plastic sheets and subjected to a pressure of 3 Bar. The plastic sheets prevented the melted GFPP samples from sticking to the hot press’ platens. The matrix of the pressed samples melted and flowed due to the applied pressure. Images of the post-heated samples are shown in Figure 2.



Figure 2. Images of post-heated (152 °C) GFPP sample, proving that melting occurs at 152 °C.

This test confirmed that the GFPP UD tape melted and flowed at 152 °C. Similar tests were performed at 150 °C and 148 °C. Limited melting and matrix flow were observed at 150 °C, but flow was not observed at 148 °C. At 148 °C, the GFPP UD tapes exhibited substantial tackiness and decreased stiffness. Accordingly, 148 °C was set as the upper processing temperature. To select the lower processing temperature limit, GFPP samples were heated in the hot press to 140, 142, 144, and 146 °C. The heated GFPP samples did not exhibit substantial tackiness below 144 °C; therefore, adequate bonding between stacked

GFPP plies is not anticipated to occur below 144 °C. Accordingly, this temperature was set as the lower processing temperature to investigate. In addition to the upper and lower temperature limits, a middle point of 146 °C was considered. Accordingly, the processing temperatures investigated were 144, 146, and 148 °C. The selected temperature range satisfies the conditions of open mold fabrication processes and practically mimics the temperature range used in ATP processes.

Identical GFPP material was successfully consolidated at a processing pressure of 10 Bar [31], though in a closed mold and at processing temperatures exceeding 150 °C. Motivated by the pressure value reported in the literature (10 Bar) [31], three pressure levels were considered to investigate the effect of processing pressure, namely 9, 10, and 11 Bar. A pressure higher than 10 Bar is considered since this work utilizes processing temperatures lower than 150 °C, and lower processing temperatures may require higher processing pressures. On the other hand, a pressure lower than 10 Bar is considered to assist in shedding light on the interactive effects of pressure, temperature, and time on ILSS, particularly as longer processing times can potentially increase the effectiveness of the processing pressure. A processing period of 5 min was found to be sufficient for fabricating laminates from identical GFPP UD tapes at temperatures exceeding 150 °C [31]. However, since the processing temperatures here are lower than 150 °C, processing periods exceeding 5 min were selected, namely 7, 10, and 13 min. Based on the selected three processing pressures, temperatures, and processing periods, the parameters test matrix shown in Table 2 is established. The effect of each combination in the test matrix on ILSS is examined.

Table 2. Process parameter test matrix.

Case No.	Temperature (°C)	Pressure (Bar)	Time (min)	Case No.	Temperature (°C)	Pressure (Bar)	Time (Min)
1	144	9	7	15	148	10	10
2	146	9	7	16	144	10	13
3	148	9	7	17	146	10	13
4	144	9	10	18	148	10	13
5	146	9	10	19	144	11	7
6	148	9	10	20	146	11	7
7	144	9	13	21	148	11	7
8	146	9	13	22	144	11	10
9	148	9	13	23	146	11	10
10	144	10	7	24	148	11	10
11	146	10	7	25	144	9	13
12	148	10	7	26	146	9	13
13	144	10	10	27	148	9	13
14	146	10	10				

The processing pressure, temperature, and time are applied following the fabrication cycle presented schematically in Figure 3. The fabrication cycle of thermoplastic laminates from plies typically involves three stages: heating, processing (dwelling), and cooling. The heating stage describes the heating period required for the plies to reach the processing temperature. The processing (dwell) stage describes the period in which the processing temperature and pressure are applied simultaneously. They are typically kept constant during this stage, hence the name dwelling stage. The duration of the processing stage (dwell stage) is called the dwell time or processing time. The cooling stage describes the period used to cool the plies from processing to room temperature. In the cooling stage, the processing pressure is released quickly.

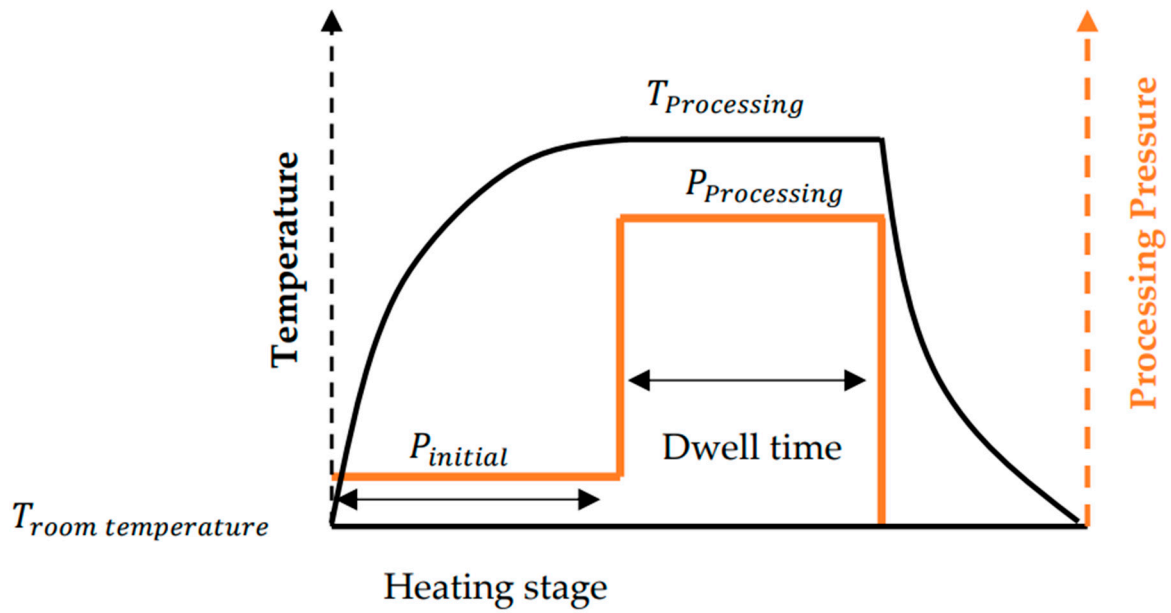


Figure 3. Processing scheme.

The fabrication cycle used in this work, as shown in Figure 3, utilizes a heating stage of 50 min. This period, found via trial and error, was sufficient for the Wabash hot press to uniformly heat a thick stack of GFPP plies (20 plies) to the selected processing temperatures. At the beginning of the heating stage, a slight pressure of 0.5 Bar was initially applied to the stacked plies to eliminate the gaps between them and facilitate heat transfer to the inner plies. This pressure was maintained throughout the heating stage. Heat was applied using the hot press' top and bottom platens. At the end of the 50 min heating phase, the stacked plies had a uniform temperature equal to the processing temperature. Temperature uniformity across the thickness of the plies was verified using a handheld infrared (IR) thermometer. In the processing stage, which follows the heating stage, the processing pressure was applied, and the processing temperature was kept constant. At the end of the processing stage, the pressure was decreased to zero, and the platens were opened. The laminate formed from the stacked plies was removed from the hot press and placed at room temperature to cool down.

Each fabrication cycle produced a unidirectional GFPP laminate consisting of 20 plies. The plies, each 10 cm long and 9 cm wide, were cut from the GFPP UD tape using a shear cutter. Each 20 plies were stacked and aligned along their fiber direction, as seen in Figure 4a. Stacked plies were placed between heat-resistant plastic sheets to prevent them from sticking to the hot press' platens and to produce a smooth surface. A stacking sequence of 20 plies was used to realize a cured unidirectional laminate with a thickness of 7 ± 0.5 mm. This thickness was used to satisfy the short beam testing protocol employed to determine the laminate's ILSS. A sample unidirectional laminate is shown in Figure 4b. Each laminate was marked and labeled. Finally, laminates were cut into short beam samples using a computer numerically controlled (CNC) machine, as seen in Figure 4c. Samples were kept in tightly sealed bags to avoid contamination and moisture effects.

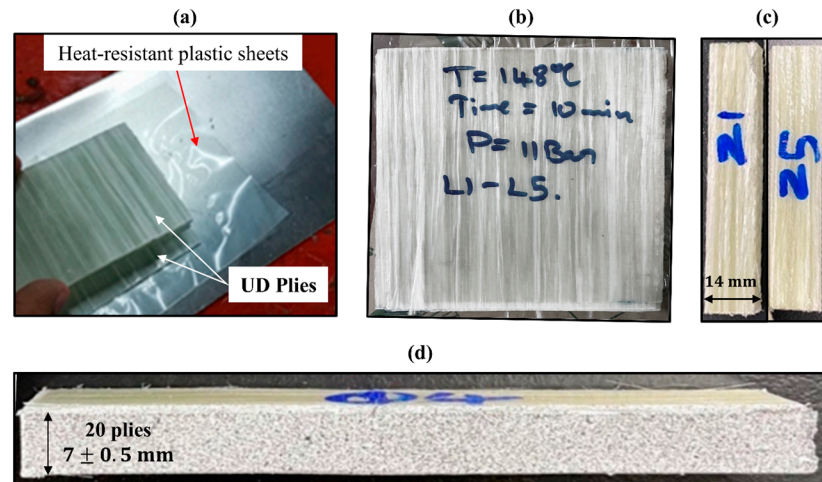


Figure 4. Sample fabrication and preparation process, showing (a) ply stacking, (b) fabricated laminate, (c) specimens cut from a laminate, and (d) specimens with a random black and white speckle pattern.

Following the standard ASTM D2344 [32], three-point bend tests were performed on the fabricated specimens to measure their interlaminar shear strength. The tests were performed using an Instron three-point-bend fixture and an Instron universal loading machine (UTM). Following the ASTM D2344 standard, the specimens’ length (between the fixed supports) and width were 6 and 2 times their thickness (~7 mm). The force and displacement of the loading roller, positioned at the midspan of the specimens’ top surface, were measured by the UTM’s load cell and internal actuator. The fixed and loading rollers of the three-point-bend loading frame had a diameter of 9 mm. Figure 5 shows a ready-to-test specimen using the three-point-bend setup. The ILSS is computed from the test using the following equation [32],

$$ILSS = 0.75 \times \frac{P_m}{b \times h} \tag{1}$$

such that P_m is the peak load, while b and h are the specimen width and thickness, respectively.

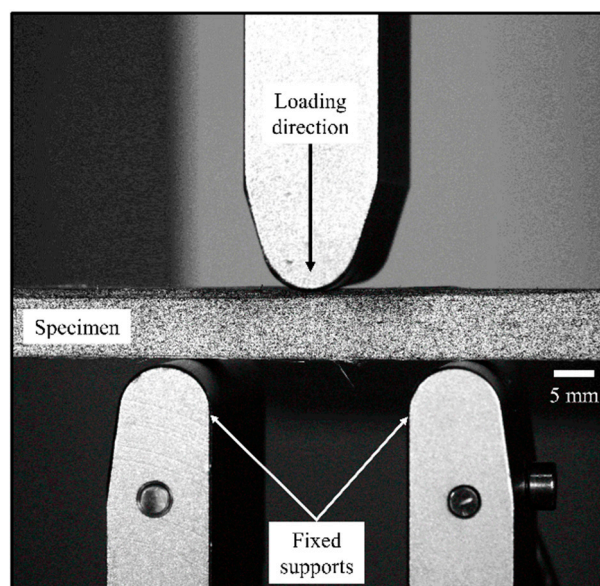


Figure 5. Specimen with speckled pattern positioned in the three-point-bend setup.

To shed light on the deformation fields inside the three-point loaded specimens, the digital image correlation (DIC) technique was used to measure the shear strains in the specimens. To this end, the specimens' sides were sprayed with random black and white patterns, as shown in Figures 4d and 5. A DIC system from Correlated Solutions, USA, was used to measure the full-field shear strains in the specimens throughout the loading process. Before spraying the paint, the surfaces of the specimens were polished using 15 μm grain size sandpaper spinning at a speed of 50 rpm. Polishing was performed to clean and even out specimens' surfaces. Moreover, polishing removed fiberglass fragments and debris induced during the cutting process of the specimens.

Microscopy was used to visually inspect the interfaces between the plies comprising the fabricated laminates. To this end, a Zeiss digital microscope was used. Specimens were investigated after they were polished before applying the black-and-white speckle pattern.

The experimental approach employing three-point bend, DIC, and microscopy allows for the measurement of specimens' macroscopic average behavior and their localized deformation fields. In addition, it provides a visual assessment of the inter-ply bond status in the fabricated specimens.

3. Results

The force–deflection curves of all 27 cases are presented in Figures 6–8, which represent cases 1~9 (i.e., pressure of 9 bar), cases 10~18 (i.e., pressure of 10 Bar) and cases 19~27 (i.e., pressure of 11 Bar), respectively. Tests that showed a drop in the loading force were stopped slightly after the force drop. All tests showed a linear loading phase that either peaked at the end of the linear phase and transitioned to a softening phase or transitioned to a quasi-plateau phase. For most cases, the force–deflection curves of the three tested specimens strongly overlapped, indicating relatively repeatable behavior.

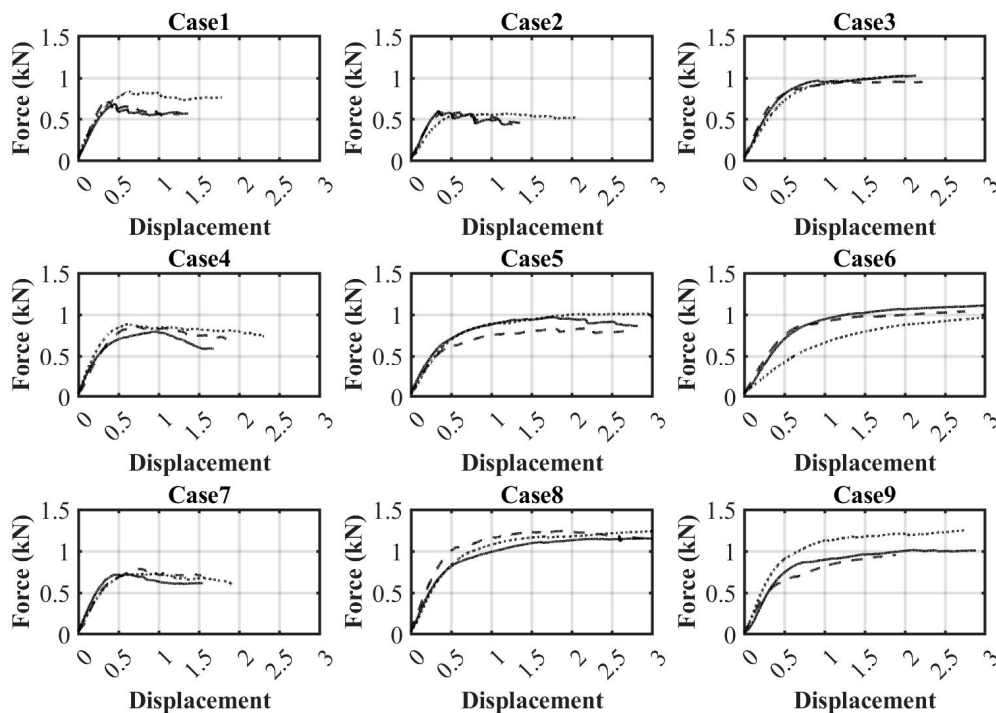


Figure 6. Force–deflection curves of cases 1~9, which used a pressure of 9 Bar. Each sub-figure shows the results of three samples such that the 1st, 2nd, and 3rd samples are represented with solid, dashed, and dotted lines, respectively.

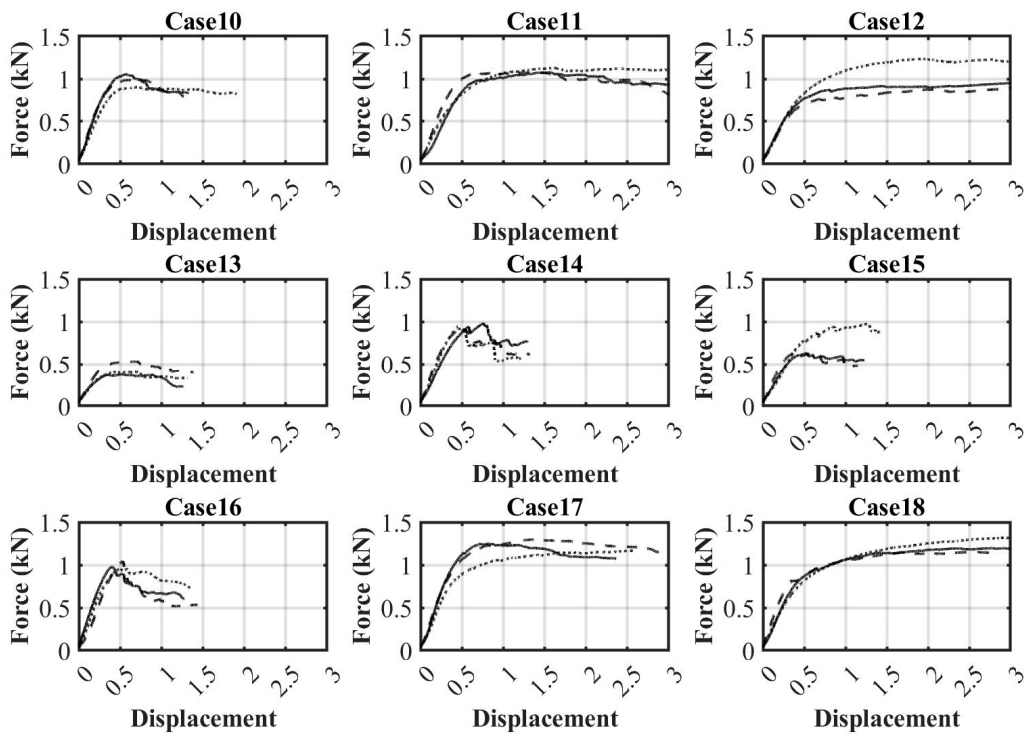


Figure 7. Force–deflection curves of cases 10~18, which used a pressure of 10 Bar. Each sub-figure shows the results of three samples such that the 1st, 2nd, and 3rd samples are represented with solid, dashed, and dotted lines, respectively.

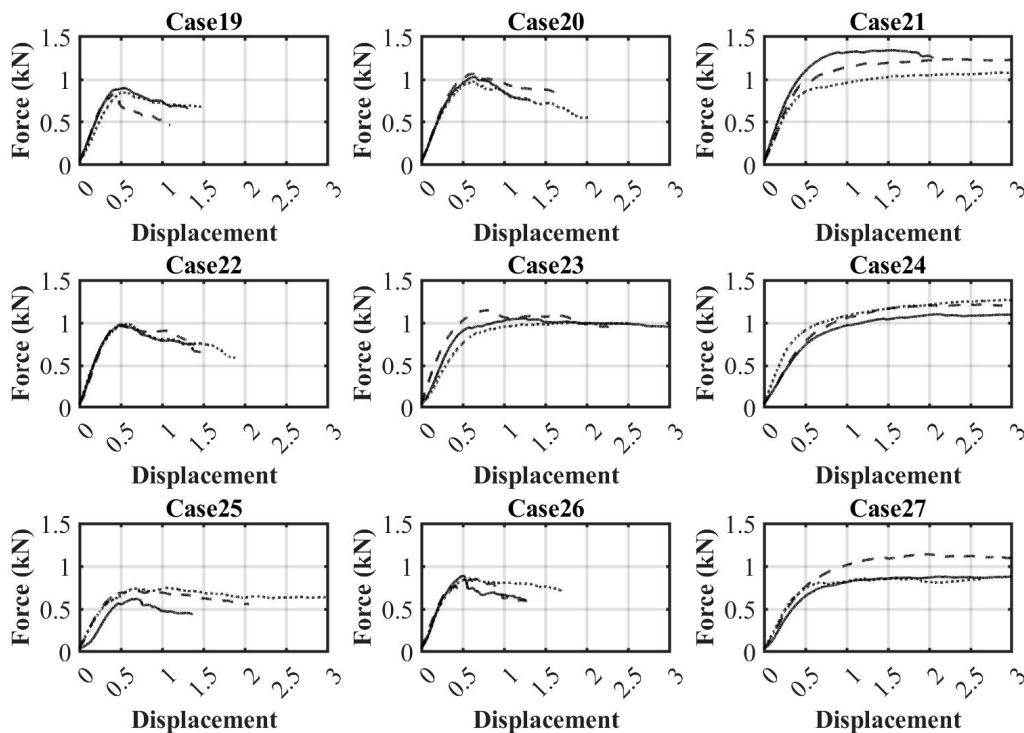


Figure 8. Force–deflection curves of cases 19~27, which used a pressure of 11 Bar. Each sub-figure shows the results of three samples such that the 1st, 2nd, and 3rd samples are represented with solid, dashed, and dotted lines, respectively.

According to the force–deflection curves, the maximum force attained by the samples corresponding to the different cases ranged approximately between ~0.5 kN and ~1 kN.

This ~100% difference is related to the difference in the achieved inter-layer bond strength. Moreover, this difference indicates that the process parameters used resulted in a wide range of bond quality.

The maximum force attained by the force–deflection curves was used to compute the ILLS using Equation (1). The resulting ILLS values for all cases are listed in Table 3. For each case, Table 3 presents the mean, highest, and lowest ILLS values. It is worth reminding that three samples were tested for each case.

Table 3. Interlaminar shear strength (ILSS).

Case	ILSS (MPa)			Case	ILSS (MPa)			Case	ILSS (MPa)		
	Mean	Highest	Lowest		Mean	Highest	Lowest		Mean	Highest	Lowest
1	4.758	5.304	4.389	10	5.991	6.434	5.486	19	5.505	5.794	5.251
2	3.749	3.858	3.667	11	7.327	7.545	7.207	20	6.818	7.061	6.435
3	6.645	6.935	6.182	12	7.304	8.838	5.943	21	8.291	9.01	7.455
4	5.228	5.465	4.935	13	3.148	3.896	2.443	22	6.499	6.568	6.383
5	7.061	7.473	6.423	14	6.929	7.043	6.816	23	7.241	7.743	6.788
6	7.965	8.32	7.553	15	5.253	6.651	4.548	24	8.417	9.046	7.634
7	4.7	4.958	4.536	16	6.205	6.519	6.006	25	4.288	4.623	3.825
8	8.51	8.82	8.044	17	8.237	8.608	7.819	26	5.761	5.795	5.705
9	8.036	9.143	7.421	18	8.347	9.107	7.885	27	6.967	8.531	6.101

The main goal of this work is to investigate the practicality of consolidating GFPP plies in an open mold process that models ATP processes. Accordingly, the cases resulting in the highest ILSS are considered the most significant to this work's goal. Cases 8 and 24 exhibited the highest mean ILSS values (8.51 MPa and 8.4 MPa, respectively). Given that the tensile strength of polypropylene is in the neighborhood of 30 MPa [33], an ILSS value of 8.5 or 8.4 MPa is considered significant. Accordingly, the results of cases 8 and 24 indicate that GFPP UD tapes can be consolidated in an open mold process. The temperature, pressure, and time corresponding to case 8 are 146 °C, 9 Bar, and 13 min, respectively. On the other hand, the temperature, pressure, and time corresponding to case 24 are 148 °C, 11 Bar, and 10 min, respectively. Accordingly, the highest ILSS values were realized with different process parameter combinations. To result in roughly the same ILSS, a more extended dwelling period (+3 min) was needed in case 8 compared to that needed for case 24 to compensate for the lower processing temperature. However, the extended dwelling time consisted of just 3 min, which is insignificant.

With respect to the lowest ILSS realized, cases 2 and 13 exhibited the lowest mean ILSS values (3.749 MPa and 3.148 MPa, respectively). The temperature, pressure, and time corresponding to cases 2 and 13 are 144 °C, 9 Bar, 7 min, and 144 °C, 10 Bar, 10 min, respectively. These results indicate that better bonding is achieved at temperatures equal to and higher than 146 °C. In addition, results highlight a significantly nonlinear and strong effect of temperature. For instance, a difference of 2 °C between 144 °C and 146 °C had a significantly higher impact than the 2 °C difference between 146 °C and 148 °C. Table 3 shows that the lowest mean ILSS values are associated with cases comprising a processing temperature of 144 °C, indicating that this temperature is unsuitable for consolidating GFPP plies in an open mold process. The small but nonzero ILSS measured values at the processing temperatures of 144 °C indicate that bonding driven by molecular diffusion occurs at this temperature at a very low and unpractical rate, too slow to realize strong interlaminar bonds. Accordingly, results indicate that a temperature of 144 °C is not a practical processing temperature.

4. Discussion

The results section presented the obtained data and emphasized the most important results, which are the cases with the highest and lowest mean ILSS. The cases with the highest ILSS demonstrated the feasibility of consolidating GFPP UD tapes in open mold

processes at temperatures below but close to their complete melting temperature. On the other hand, the cases with the lowest ILSS showed that temperature is the most critical processing parameter and highlighted the lower feasible temperature bound. They demonstrated that 146 °C and 148 °C processing temperatures provide a significantly better prospect for realizing interlaminar bonds than does the processing temperature of 142 °C. The results section successfully demonstrated the feasibility of the open mold process using a macroscopic approach that assessed the specimens through their force-displacement curves and ILLS values. However, the results are discussed here from four additional perspectives: the internal response and deformation fields within specimens, microscopy and images of the bonded interfaces, the interaction of the process parameters, and the potential of open mold processes compared to that of conventional closed model processes.

The shear strain fields were measured in each sample during its entire loading history. Images were captured at a rate of one per second; thus, they covered all stages of the loading process. Most samples exhibited qualitatively similar shear strain fields. Representative shear strain fields corresponding to sample 2 of case 11 are shown in Figure 9. This figure shows the shear strain field at different loading stages. The strain fields are relatively symmetric, but their distribution differs from the theoretical one. Theoretically, the maximum shear strain should occur along the bending neutral axis (i.e., mid-plane), and the shear strain should follow a continuous parabolic distribution. However, the shear strain fields measured experimentally did not follow a parabolic distribution, as can be inferred from Figure 9. To quantify the shear strain distribution, its variation along two lines was determined from the DIC software (version number 9), as shown in Figure 10.

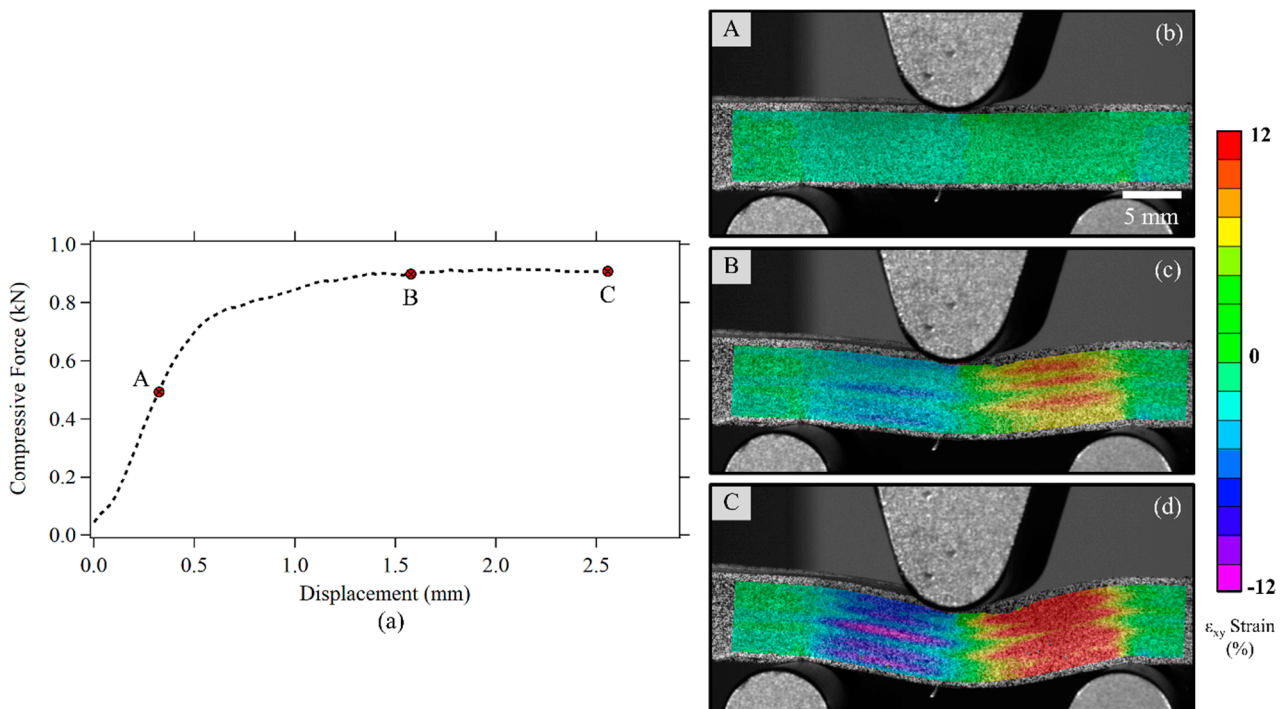


Figure 9. Full-field shear strains in sample 2 of case 11 at different loading stages. (a) The force-displacement response, (b) the strain distribution at the middle of the linear force-displacement phase, and (c,d) the strain distribution at peak and after peak load, respectively.

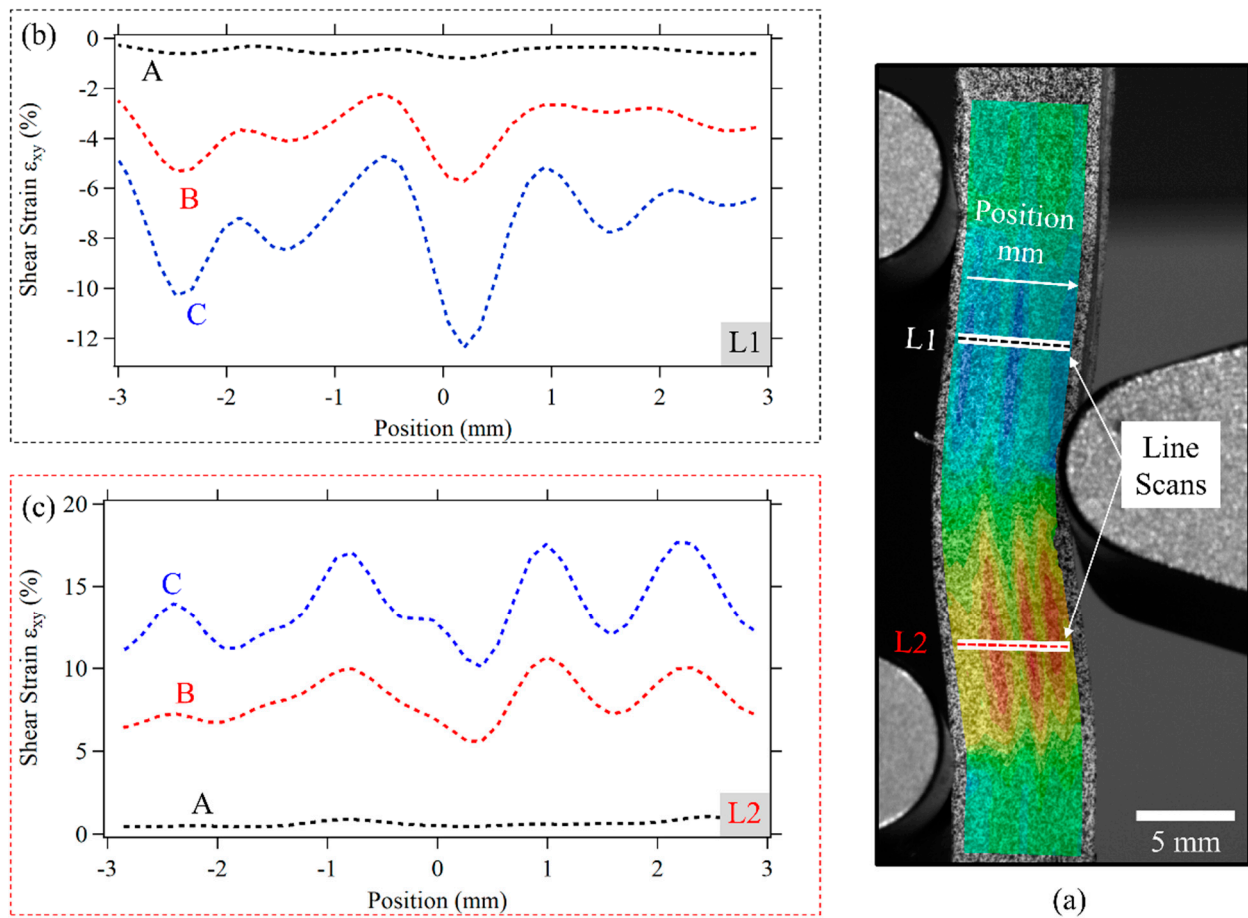


Figure 10. Shear strain distribution at different loading stages. (a) The location at which the shear strain is measured, and (b,c) the shear strain distribution at locations L1 and L2, respectively. A, B, and C correspond to the loading stages shown in Figure 9.

Figure 10 shows that the shear strain distribution at the two locations is relatively symmetric until the peak load. However, at the location marked by L2, the shear strain reaches higher magnitudes at loading stages beyond the peak load. Moreover, Figure 10 shows that the shear strain distribution does not follow the theoretically predicted parabolic relation. Shear strain distribution followed a fluctuating profile and exhibited significantly high shear strains at locations above and below the mid-plane. This difference between the predicted and measured shear strain distribution is related to the simplifying assumptions included in the theoretical predictions, which ignore the effect of loading rollers, material spatial heterogeneity (e.g., distribution of matrix, fibers, and fiber-matrix interfaces), and their interaction with force transmission lines within the tested specimens [34]. The force transmission lines within the short beam samples cause significantly large shear strains in areas located at the right and left of the middle roller, not directly below it. The high shear strain areas occupy regions that start above the mid-plane and end below it. Finite element modeling of the short beam three-point-bend test showed these high shear strain regions and demonstrated that they follow a wing profile due to their symmetry [34]. The difference between the distribution of the measured shear strains and the theoretical one affects the accuracy of the predicted ILSS values [34–36]. Errors exceeding 5% were reported in carbon fiber-based laminates [35]. Such errors could increase for laminates with lower stiffness. Defects and stress concentrations induced by spatial heterogeneities in locations above or below the mid-plane could trigger failure in the loaded specimens as these locations experience high stress levels. This scenario differs from the theoretical one, which assumes failure occurs at the mid-plane (i.e., location of highest shear stress). Accordingly, the ILSS values theoretically predicted using Equation (1) could underestimate the real values. It is

important to acknowledge this error and understand its level and source. However, since the documented errors associated with theoretically predicted ILSS values obtained using short beam three-point-bend test are in the order of 5% [35], the theoretically predicted ILSS values are considered practically accurate for this work.

Measured ILSS values exhibited some scatter, which can be attributed to the interaction of the randomly distributed defects and heterogeneities with the large shear strains in areas afar from the mid-plane. To minimize the effect of scatter, three specimens were tested per case. For most cases, the difference between the absolute maximum ILSS value and the mean was less than 10%. The scatter in ILSS values is much higher than the scatter in the force–displacement curves. Unlike force–displacement curves, which represent overall homogenized behavior, ILSS is driven by the interaction of critically weak points with high stresses. Accordingly, ILSS values can exhibit more scatter than can force–displacement curves.

The microstructure of the tested data can shed more light on the mechanisms contributing to the scatter in the ILSS values and the quality of the established interlaminar bonds. Representative samples corresponding to each case were investigated using optical microscopy prior to mechanical testing. In most cases, defects at the interlaminar interfaces were observed at the microstructure level. To illustrate these interlaminar defects, the microstructure of a sample corresponding to case 13 is shown in Figure 10.

This figure shows the microstructure at two locations in the same sample. At the first location (Figure 11a), a large defect can be seen, but it is discontinuous and ends at the left of the image in an area where a proper bond is established. Moreover, around the defect, few bridging connections were observed. However, in the same sample, the microstructure at the second location (Figure 11b) did not exhibit observable inter-ply bonding defects. Accordingly, Figure 11 suggests that inter-ply defects are distributed across the bonded specimens. Characterizing the statistical distribution of bonding defects would be valuable but is considered beyond the scope of this work, particularly as it requires specialized tools (e.g., micro-CT scan) to measure the three-dimensional distribution of defects. It is worth noting that the microstructure in Figure 11 is for a sample cured at 144 °C, which is the lowest temperature considered in this work. This sample was selected to show that bonding occurred at multiple locations, even at the lower bound of the temperatures used. Microstructures of samples processed at higher temperatures included significantly fewer observable defects.

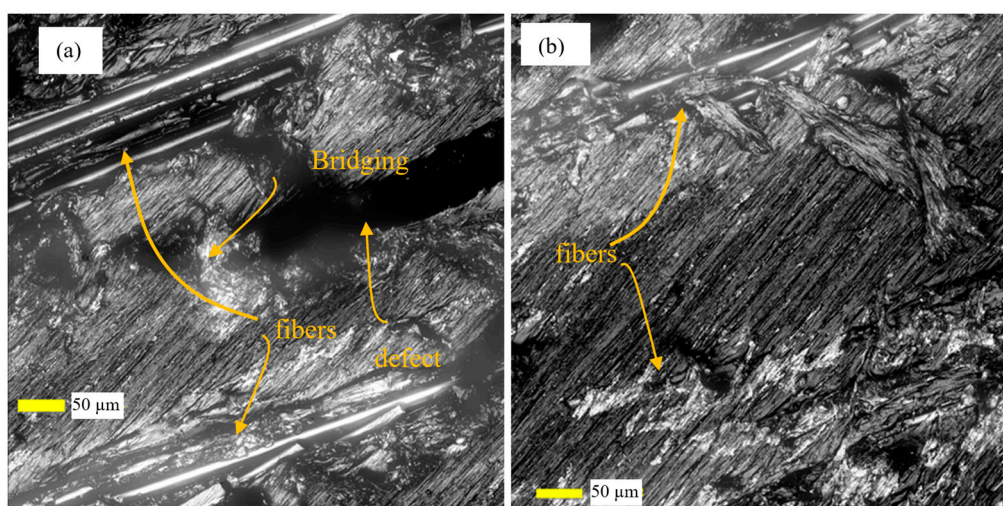


Figure 11. Optical microscopy images showing the microstructure in a representative sample corresponding to case 13 at two different locations. Location (a) presents a compromised bond, while location (b) presents a better bond at the interlayer interface.

One of the objectives of this work is to assess the interactive and hard-to-anticipate effects of the process parameters on ILSS. Analysis of variance (ANOVA) is used to assess the level of influence of the investigated process parameters and highlight their interactive effects. This analysis is essential to understanding the dependence of ILSS values on the process parameters, particularly for cases not associated with the highest and lowest observed ILSS values. Using Minitab software (version number 19), a full factorial design $(3)^3$ is used to test the significance of temperature, pressure, and time on ILSS. Although full factorial design is more tedious than other designs like Taguchi and fractional factorial, it is more informative and efficient [37]. Full Factorial design provides a means for testing interactions between the considered factors. Table 2 shows all possible combinations of the three factors at three different levels. Table 3 shows the ILSS results of the 27 experiments, considering three replicates of each experiment. Figure 12 shows the residual plots of the ANOVA analysis, utilizing all 27 experiments listed in Table 3. The residual plots confirm the normality and constant variance of the tested results (i.e., ILSS values).

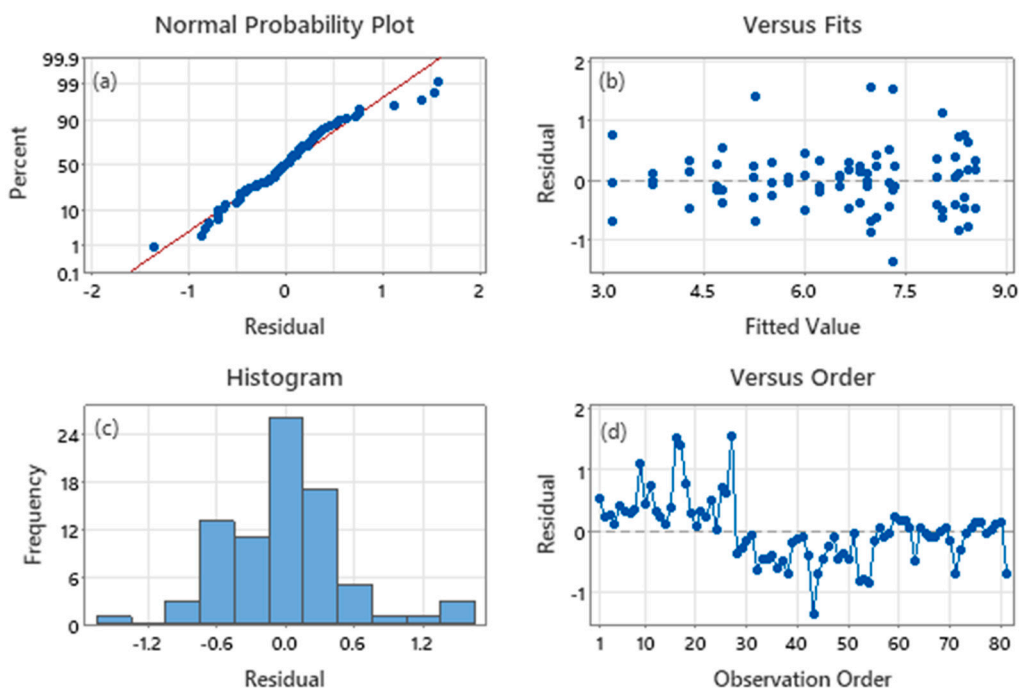


Figure 12. Residual plots from the ANOVA analysis, showing a (a) normal probability plot, (b) residual vs. fit plot, (c) residual histogram, and (d) the residual vs. observation order.

Table 4. Analysis of variance results.

Source	Contribution	p-Value
P (Pressure)	0.85%	0.128
T (Temperature)	38.99%	0.000
S (Time)	1.92%	0.012
P × T	4.67%	0.001
P × S	30.42%	0.000
T × S	5.03%	0.000
P × T × S	7.42%	0.000
Error	10.71%	
Total	100.00%	

ANOVA analysis based on a 95% confidence interval (CI) is implemented to determine the significance of each process parameter based on its *p*-value. Table 4 shows that all factors, except pressure, and their interactions significantly affect ILSS. Temperature has the highest

contribution, with 38.99%. Although pressure has no significant effect as a standalone process parameter, the interactions of pressure–time, pressure–temperature, and pressure–temperature–time are considered significant with a p -value $\ll 0.05$. The contribution of pressure and its interactions is 43.36%. Accordingly, pressure is a considerable parameter and cannot be ignored, although it has a p -value > 0.05 .

This work attempted to use regression to establish a mathematical relationship between ILSS and process parameters. Such a relationship can help predict the ILSS corresponding to given process parameter values. However, according to the conducted statistical analysis (i.e., using Minitab), the best regression relating ILSS to the process parameters had a coefficient of determination (R^2) of ~ 0.6 , indicating that regression could not fully capture the relationship between ILSS and the process parameters. The inability of regression to provide a predictive relationship motivated the use of artificial intelligence tools.

An adaptive neuro-fuzzy inference system (ANFIS) [38] was used to capture the relationship between ILSS and the process parameters. The proposed ANFIS was trained and developed using the NEURO-FUZZY toolbox available in MATLAB. Figure 13 shows the architecture of the used ANFIS. It has the standard five-layer ANFIS architecture. The first layer comprises the inputs, which are the three process parameters. The temperature, pressure, and time are named input 1, 2, and 3, respectively. The output layer represents the ILSS value. In the second layer, Gaussian membership functions were used to transform the input values into equivalent fuzzy values. Three membership functions were used to handle each temperature and pressure, while two were used to handle time. Figure 14 shows the input membership functions. The following layer comprises the fuzzy rules to be fired from the expert system using TSK fuzzy rules. In total, 18 rules were used based on the grid partition of the given data. Similarly, 18 output membership functions were used in the fourth layer to start the defuzzification process of the output. In the last layer, the normalized weights of the defuzzified outputs were summed to provide the ANFIS's output (i.e., ILSS). A hybrid ANFIS learning algorithm was used to tune the output weights of the rules, inputs, and the membership functions' parameters to reduce the mean squared error between the actual ILSS values and the predicted output values [39]. Briefly, 65% of the data were used for training, 20% were used for testing, and 15% were used for validating the ANFIS model.

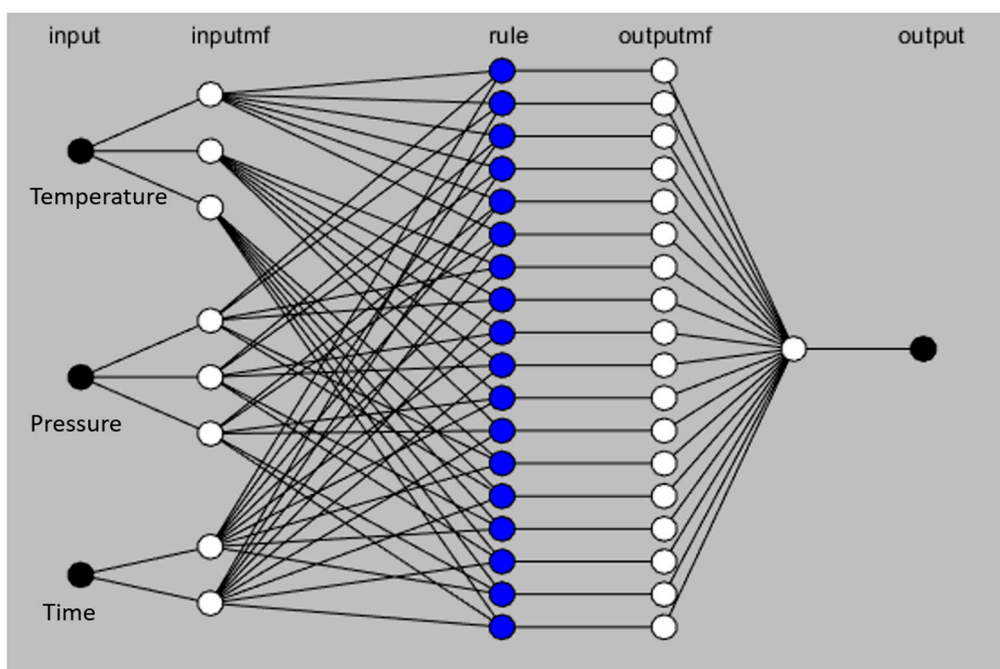


Figure 13. ANFIS architecture.

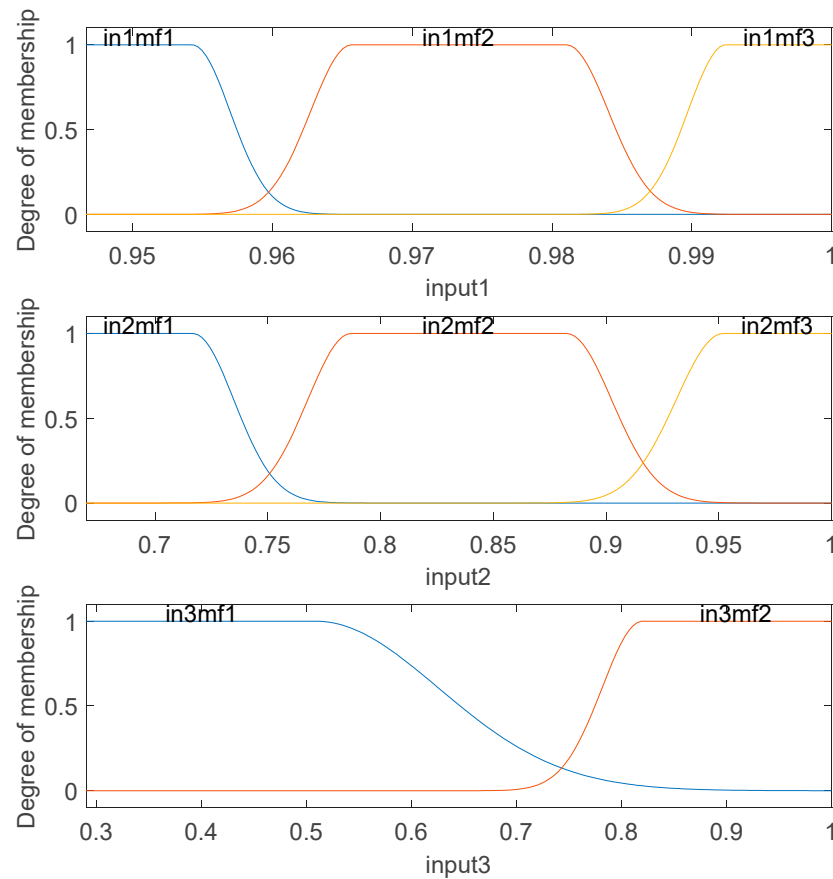


Figure 14. Input variable membership functions.

Figure 15 demonstrates the performance of the developed ANFIS model in capturing the relationship between process parameters and ILSS. This figure shows the linear regression plots of the complete, training, testing, and validation sets. Regression plots show that the ANFIS model efficiently captures the relationship between ILSS and process parameters. The efficiency of the ANFIS model was also investigated by computing the coefficient of determination, R^2 , and the mean squared error, MSE, for each set. The resulting values are reported in Table 5. The R^2 values and the small MSE values shown in Table 5 confirm the accuracy of the developed ANFIS model. An analysis of the ANFIS model performance, using Figure 15 and Table 5, demonstrates the predictive potential of the developed ANFIS. The model can predict the ILSS values corresponding to different combinations of process parameters. Accordingly, although regression could not capture the ILSS–process parameters relationship, artificial intelligence tools, namely adaptive neuro-fuzzy inference systems, could capture the relationship. This outcome satisfies one of the goals of this work, which aims to establish predictive models that relate ILSS to process parameters. Such models can benefit engineers in the development cycle and fabrication of composites.

Table 5. Performance indicators describing the accuracy of the ANFIS Model.

	Coefficient of Determination (R^2)	Mean Squared Error MSE
Training Set	0.9593	0.0799
Testing Set	0.7188	0.6609
Validating Set	0.8213	0.4114
Complete Set	0.8807	0.2459

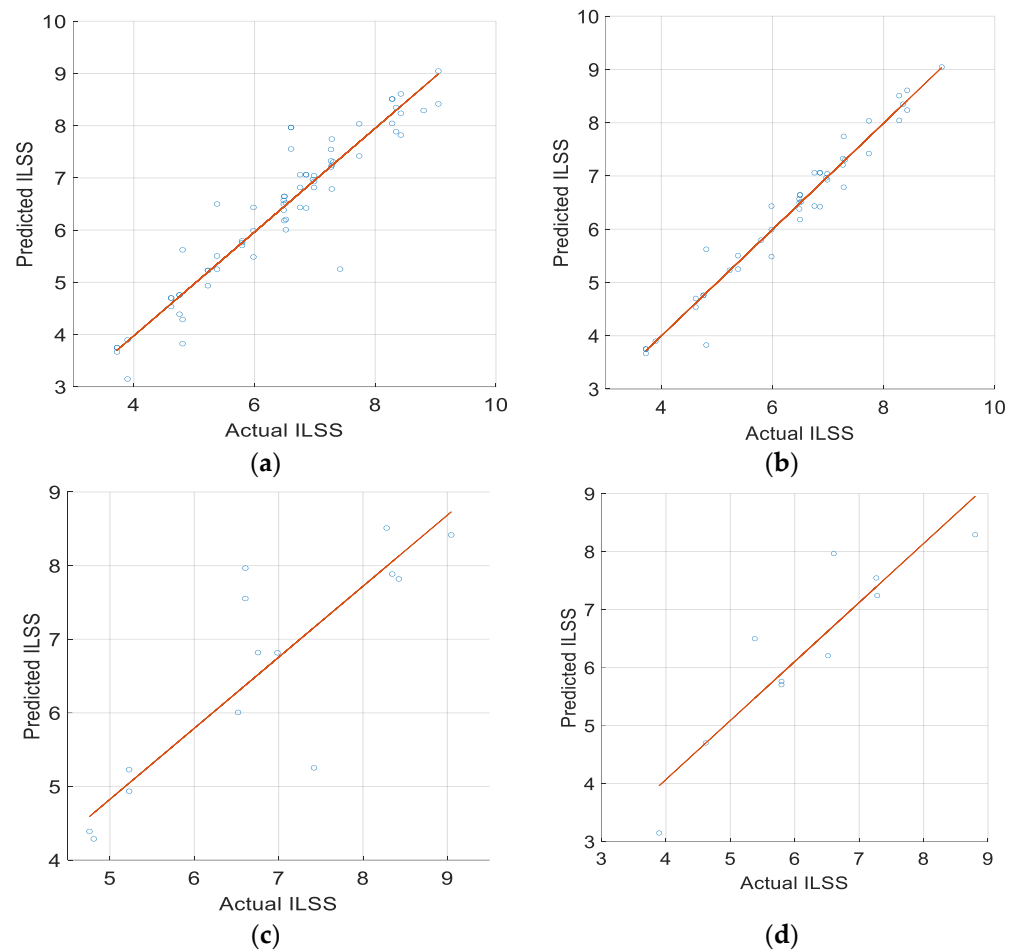


Figure 15. Linear regression plots of (a) complete set, (b) training set, (c) testing set, and (d) validating set.

The developed ANFIS model was used to search, by using interpolation, for the processing temperature and time combinations that result in the highest ILSS values at each of the pressures: 9 Bar, 10 Bar, and 11 Bar. At 9 Bar, the ANFIS predicts that the highest ILSS values are obtained at a processing time of 13 min and at a processing temperature between 146 °C and 147 °C. At 10 Bar, the highest ILSS values are obtained at a processing time of 12.5–13 min and at a processing temperature between 146 °C and 148 °C. Finally, at 11 Bar, the highest ILSS values are obtained at a processing time below 11 min and at a temperature between 146.5 °C and 148 °C. These predictions highlight interesting behavior. Longer processing time assists in obtaining higher ILSS values at the pressures of 9 and 10 Bars. Conversely, a longer processing time exceeding 11 min at the pressure of 11 Bars resulted in reduced ILSS values. This behavior implies that a processing pressure of 11 Bar is too high, and applying it for more extended periods can induce damage to the processed laminate. Moreover, the results of the ANFIS imply that processing times exceeding 13 min at a processing pressure of 9 and 10 bars could result in an even higher ILSS than that observed in this work.

Finally, the results of this work confirmed the feasibility of processing GFPP UD in open mold-based processes. However, following this processing route is associated with costs that should be considered. The process itself is governed by interactive process parameters that can complicate the control of the fabrication process. Moreover, laminates produced by this process can exhibit reduced ILSS values compared to those processed using closed mold techniques in which the laminates melt entirely during processing. The ILSS of GFPP laminates fabricated using classical techniques have been reported to reach more than double the ILSS values achieved in this work [40]. This difference does not

undermine the feasibility and practicality of open mold processes, but it underscores the need to assess the advantages and disadvantages of this processing technique before using it. This argument applies to both open and closed mold processes as open mold processes facilitate the automation of the processing of large parts (e.g., using tape placement), while closed mold processes provide superior properties and are easier to control.

5. Conclusions

The feasibility of processing GFPP UD tapes in an open mold process at temperatures very close to but below their matrices' complete melting and flow temperature was assessed experimentally. To this end, unidirectional laminates were fabricated from GFPP UD tapes using multiple temperatures, pressures, and processing times. The quality of the inter-ply bond formed during processing was assessed by measuring the ILSS of the fabricated specimens using the short-beam three-point-bend test in conjunction with the 3D image correlation technique. The highest ILSS values obtained, slightly exceeding 8 MPa, demonstrated the feasibility of processing GFPP UD tapes in open mold processes. Analysis of variance was performed to examine the relationship between ILSS and the processing parameters. The standalone effect of temperature and the interactive effects of pressure–time, pressure–temperature, and pressure–time–temperature contributed the most to the relationship between the ILSS and process parameters. Due to its dependence on interactive terms, the relationship between the ILSS and process parameters can be classified as nonlinear. The distribution of shear strain, which was measured using image correlation, in the tested specimens differed from the theoretical one. Measured shear strain fields did not follow a parabolic distribution and exhibited high values at locations afar from samples' mid-planes. The interaction of defects and stress concentration induced by spatial heterogeneities caused a failure to start at locations above or below the location of the theoretical maximum shear stress. The latter introduced scatter in the measured ILSS values. Compared to conventional closed model processing techniques for thermoplastic UD tapes, the examined open-mode method results in lower ILSS values (approximately lower by 50%). Though open methods have an advantage over conventional closed methods in terms of facilitating automation and increasing throughput, they can produce inferior laminates. Accordingly, users should consider the advantages and limitations of both processing techniques before selecting one for a particular application. Results showed that the relationship between ILSS and process parameters is complex and could not be described using regular regression. However, advanced artificial intelligence tools, namely adaptive neuro-fuzzy inference systems (ANFS), proved efficient and accurate in modeling the ILSS–process parameters relationship. The ANFIS model showed that processing pressures exceeding 10 Bar might not improve processed laminates' ILSS and implied that increasing the processing time at the pressures of 9 and 10 Bars can improve laminates' ILSS.

Author Contributions: Conceptualization, M.A. and W.A.; methodology, M.A., W.A. and M.A.J.; formal analysis, B.A., K.K. and M.M.; investigation, B.A. and M.H.; resources, M.A., W.A. and M.A.J.; data curation, B.A. and M.A.; writing—original draft preparation, M.A., M.A.J. and M.M.; writing—review and editing, W.A. and K.K.; visualization, K.K., M.M. and W.A.; supervision, M.A. and W.A.; project administration, M.A.; funding acquisition, M.A. All authors have read and agreed to the published version of the manuscript.

Funding: This research was funded by The American University of Sharjah FRG Program, grant number FRG23-E-E41. The APC was funded by The American University of Sharjah Open Access Program. This paper represents the opinions of the author(s) and does not mean to represent the position or opinions of the American University of Sharjah.

Data Availability Statement: Data are included in the article. Additionally, data presented in this study are available in digital form on request from the corresponding author.

Acknowledgments: This work was funded by the American University of Sharjah under grant FRG23-E-E41. This paper represents the opinions of the author(s) and does not mean to represent the position or opinions of the American University of Sharjah.

Conflicts of Interest: The authors declare no conflicts of interest.

References

1. Chawla, K.K. *Composite Materials: Science and Engineering*; Springer: Cham, Switzerland, 2019.
2. Kaw, A.K. *Mechanics of Composite Materials*; CRC Press: Boca Raton, FL, USA, 2005.
3. Afshar, A.; Alkhader, M.; Korach, C.S.; Chiang, F.-P. Effect of long-term exposure to marine environments on the flexural properties of carbon fiber vinylester composites. *Compos. Struct.* **2015**, *126*, 72–77. [[CrossRef](#)]
4. Elyoussef, M.; Abuzaid, W.; Alkhader, M. Experimental assessment of temperature effect on open-hole notch sensitivity in woven carbon fiber composites. *Arch. Appl. Mech.* **2020**, *91*, 1273–1290. [[CrossRef](#)]
5. Afshar, A.; Alkhader, M.; Korach, C.S.; Chiang, F.-P. Synergistic Effects of Fatigue and Marine Environments on Carbon Fiber Vinyl-Ester Composites. *J. Eng. Mater. Technol.* **2015**, *137*, 041002. [[CrossRef](#)]
6. Mazumdar, S. *Composites Manufacturing: Materials, Product, and Process Engineering*; CRC Press: Boca Raton, FL, USA, 2001.
7. Abderrafai, Y.; Diouf-Lewis, A.; Sosa-Rey, F.; Farahani, R.D.; Piccirelli, N.; Lévesque, M.; Therriault, D. Additive manufacturing and characterization of high temperature thermoplastic blends for potential aerospace applications. *Compos. Sci. Technol.* **2023**, *231*, 109839. [[CrossRef](#)]
8. Hanemann, T.; Klein, A.; Baumgärtner, S.; Jung, J.; Wilhelm, D.; Antusch, S. Material Extrusion 3D Printing of PEEK-Based Composites. *Polymers* **2023**, *15*, 3412. [[CrossRef](#)]
9. Favaloro, M. A Comparison of the Environmental Attributes of Thermoplastic vs. Thermoset Composites. In Proceedings of the International SAMPE Technical Conference, Wichita, KS, USA, 19–22 October 2009.
10. Harutun, K. *Handbook of Polypropylene and Polypropylene Composites, Revised and Expanded*; CRC Press: Boca Raton, FL, USA, 2003.
11. Richardson, M.O.W.; Wisheart, M.J. Review of low-velocity impact properties of composite materials. *Compos. Part A Appl. Sci. Manuf.* **1996**, *27*, 1123–1131. [[CrossRef](#)]
12. Steenkamer, A.D.; Sullivan, J.L. On the recyclability of a cyclic thermoplastic composite material. *Compos. B Eng.* **1998**, *29*, 745–752. [[CrossRef](#)]
13. Hulcher, A.B.; McGowan, D.M.; Grimsley, B.W.; Johnston, N.J.; Gordon, G.H. *Processing and Testing of Thermoplastic Composite Cylindrical Shells Fabricated by Automated Fiber Placement*; NASA: Washington, DC, USA, 2001.
14. Qureshi, Z.; Swait, T.; Scaife, R.; El-Dessouky, H. In situ consolidation of thermoplastic prepreg tape using automated tape placement technology: Potential and possibilities. *Compos. B Eng.* **2014**, *66*, 255–267. [[CrossRef](#)]
15. Brasington, A.; Sacco, C.; Halbritter, J.; Wehbe, R.; Harik, R. Automated fiber placement: A review of history, current technologies, and future paths forward. *Compos. Part C Open Access* **2021**, *6*, 100182. [[CrossRef](#)]
16. Potter, K. Automated Fibre Placement. In *Design and Manufacture of Structural Composites*; Elsevier: Amsterdam, The Netherlands, 2023; pp. 125–143.
17. Sonmez, F.O.; Akbulut, M. Process optimization of tape placement for thermoplastic composites. *Compos. Part A Appl. Sci. Manuf.* **2007**, *38*, 2013–2023. [[CrossRef](#)]
18. Venkatesan, C.; Zulkifli, F.; Silva, A. Effects of processing parameters of infrared-based automated fiber placement on mechanical performance of carbon fiber-reinforced thermoplastic composite. *Compos. Struct.* **2023**, *309*, 116725. [[CrossRef](#)]
19. Oromiehie, E.; Gain, A.K.; Prusty, B.G. Processing parameter optimisation for automated fibre placement (AFP) manufactured thermoplastic composites. *Compos. Struct.* **2021**, *272*, 114223. [[CrossRef](#)]
20. Pitchumani, R.; Ranganathan, S.; Don, R.C.; Gillespie, J.W., Jr.; Lamontia, M.A. Analysis of transport phenomena governing interfacial bonding and void dynamics during thermoplastic tow-placement. *Int. J. Heat Mass Transf.* **1996**, *39*, 1883–1897. [[CrossRef](#)]
21. Schledjewski, R.; Latrille, M. Processing of unidirectional fiber reinforced tapes—Fundamentals on the way to a process simulation tool (ProSimFRT). *Compos. Sci. Technol.* **2003**, *63*, 2111–2118. [[CrossRef](#)]
22. Liu, L.; Hu, D.; Zhang, Y.; Han, X. Experimental research on the mechanism of non-monotonic characteristic between curing temperature and mechanical behaviors of Kevlar/epoxy composite. *Sci. China Technol. Sci.* **2018**, *61*, 1012–1020. [[CrossRef](#)]
23. Van de Velde, K.; Kiekens, P. Effect of material and process parameters on the mechanical properties of unidirectional and multidirectional flax/polypropylene composites. *Compos. Struct.* **2003**, *62*, 443–448. [[CrossRef](#)]
24. Perrin, F.; Bureau, M.; Denault, J.; Dickson, J. Mode I interlaminar crack propagation in continuous glass fiber/polypropylene composites: Temperature and molding condition dependence. *Compos. Sci. Technol.* **2003**, *63*, 597–607. [[CrossRef](#)]
25. Chen, Q.; Boisse, P.; Park, C.H.; Saouab, A.; Bréard, J. Intra/inter-ply shear behaviors of continuous fiber reinforced thermoplastic composites in thermoforming processes. *Compos. Struct.* **2011**, *93*, 1692–1703. [[CrossRef](#)]
26. Lang, D.; Barre, S.; Coiffier-Colas, C.; Sibois, H. Thermoplastic Tape Placement and Continuous Consolidation. In Proceedings of the RTO AVT Specialists' Meeting on "Low Cost Composite Structures, Loen, Norway, 7–11 May 2001.
27. Nayak, R.K.; Rathore, D.; Ray, B.; Routara, B. Inter laminar shear strength (ILSS) of nano Al₂O₃ filled glass fiber reinforced polymer (GFRP) composite—A study on loading rate sensitivity. *Mater. Today Proc.* **2017**, *4*, 8688–8696. [[CrossRef](#)]

28. Ahmed, K.S.; Vijayarangan, S. Tensile, flexural and interlaminar shear properties of woven jute and jute-glass fabric reinforced polyester composites. *J. Mater. Process. Technol.* **2008**, *207*, 330–335. [[CrossRef](#)]
29. Fan, Z.; Santare, M.H.; Advani, S.G. Interlaminar shear strength of glass fiber reinforced epoxy composites enhanced with multi-walled carbon nanotubes. *Compos. A Appl. Sci. Manuf.* **2008**, *39*, 540–554. [[CrossRef](#)]
30. Tiganis, B.E.; Shanks, R.A.; Long, Y. Effects of Processing on the Microstructure, Melting Behavior, and Equilibrium Melting Temperature of Polypropylene. *J. Appl. Polym. Sci.* **1996**, *59*, 663–671. [[CrossRef](#)]
31. Kabbani, M.S.; A El Kadi, H. Predicting the effect of cooling rate on the mechanical properties of glass fiber–polypropylene composites using artificial neural networks. *J. Thermoplast. Compos. Mater.* **2018**, *32*, 1268–1281. [[CrossRef](#)]
32. *D2344*; Annual Book of ASTM Standards. American Society for Testing and Materials: Philadelphia, PA, USA, 2013.
33. Embabi, M.; Kweon, M.S.; Chen, Z.; Lee, P.C. Tunable Tensile Properties of Polypropylene and Polyethylene Terephthalate Fibrillar Blends through Micro-/Nanolayered Extrusion Technology. *Polymers* **2020**, *12*, 2585. [[CrossRef](#)] [[PubMed](#)]
34. Allott, N.R.; Czabaj, M.W. Characterization of the interlaminar shear strength of IM7/8552 using small-scale short beam shear tests. *Compos. A Appl. Sci. Manuf.* **2020**, *142*, 106200. [[CrossRef](#)]
35. Abali, F.; Pora, A.; Shivakumar, K. Modified Short Beam Shear Test for Measurement of Interlaminar Shear Strength of Composites. *J. Compos. Mater.* **2003**, *37*, 453–464. [[CrossRef](#)]
36. Liu, C.; Du, D.; Li, H.; Hu, Y.; Xu, Y.; Tian, J.; Tao, G.; Tao, J. Interlaminar failure behavior of GLARE laminates under short-beam three-point-bending load. *Compos. B Eng.* **2016**, *97*, 361–367. [[CrossRef](#)]
37. Montgomery, D.C. *Design and Analysis of Experiments*; John and Wiley and Sons: Hoboken, NJ, USA, 2017.
38. Jang, J.-S.R. ANFIS: Adaptive-Network-Based Fuzzy Inference System. *IEEE Trans. Syst. Man Cybern.* **1993**, *23*, 665–685. [[CrossRef](#)]
39. Khasawneh, N.; Jaradat, M.A.K.; Fraiwan, L.; Al-Fandi, M. Adaptive neuro-fuzzy inference system for automatic sleep multistage level scoring employing EEG, EOG, and EMG extracted features. *Appl. Artif. Intell.* **2011**, *25*, 163–179. [[CrossRef](#)]
40. Lee, I.-G.; Kim, D.-H.; Jung, K.-H.; Kim, H.-J.; Kim, H.-S. Effect of the cooling rate on the mechanical properties of glass fiber reinforced thermoplastic composites. *Compos. Struct.* **2017**, *177*, 28–37. [[CrossRef](#)]

Disclaimer/Publisher’s Note: The statements, opinions and data contained in all publications are solely those of the individual author(s) and contributor(s) and not of MDPI and/or the editor(s). MDPI and/or the editor(s) disclaim responsibility for any injury to people or property resulting from any ideas, methods, instructions or products referred to in the content.